PROGRESS IN COLOR, COLORANTS AND COATINGS

available online @ www.pccc.icrc.ac.ir

Progress in Color Colorants Coating 20 (2027), 221-236

Ministry of Science, Research and Technology
Institute for Color Science & Technology

Titanium Metallic Additives for Enhanced Thermal Stablity and Heat Barrier Performance of Bio-based Epoxy for Potential Coating Applications

M. Abdulazeez, N. Acaralı*

Department of Chemical Engineering, Yildiz Technical University, P.O. Box: 34220, Istanbul, Türkiye

ARTICLE INFO

Article history:
Received: 21 May 2026
Final Revised: 12 Jul 2026
Accepted: 16 Jul 2026
Available online: 07 Sep 2026

Keywords:
Castor oil
Titanium metallic
Epoxy resin
White aqueous pigment

ABSTRACT

Protective coatings played an important role in surface protection and in enhancing the visual appearance of coated substrates. In this study, the factors influencing the development of highly glossy coating systems, designed to achieve optimized optical, thermal, and morphological performance, were investigated. The study focused on developing adaptive surfaces by incorporating white aqueous pigments, castor oil, and titanium metallic particles into an epoxy resin matrix applied on aluminium substrates. A systematic evaluation of additive concentrations was carried out to achieve controlled dispersion and improved visual appearance. Infrared thermography, gloss measurements, colorimetry, contact angle analysis, and TG/DTA techniques were used for characterization. The results indicated that the optimized formulation influenced both surface and thermal properties. Infrared analysis showed variations in heat distribution among epoxy-based samples, while gloss measurements suggested that samples with lower temperature fluctuations tended to exhibit higher gloss values, indicating improved surface uniformity. Surface energy analysis revealed a transition from the reference surface condition (contact angle: 65.20°) to a more hydrophilic optimized condition (contact angle: 48.38°), suggesting an increase in surface wettability. TG/DTA results showed that the addition of titanium metallic particles increased the residual mass at 600 °C, indicating enhanced thermal stability and increased char formation rather than complete thermal degradation of the material. Overall, the optimized coating system demonstrated improved combined thermal, optical, and surface properties, providing a promising approach for multi-functional coating applications. Prog Color Colorants Coat. 20 (2027), 221-236© Institute for Color Science and Technology.

1. Introduction

Liquid repellency and anti-fouling performance [1-4], wear resistance [5], and corrosion resistance enabled their wide application in various optical and engineering fields such as glass production [6]. In addition, wear resistance and tribological properties [7, 8], as well as ultraviolet (UV) resistance, were among the key characteristics of multifunctional anti-fouling coatings [9]. These systems were widely used in marine engineering and public infrastructure. For instance, curtain wall systems in high-rise buildings imposed strict requirements on multifunctional glass coatings, including high transparency, UV resistance, high hardness, and excellent anti-fouling performance to withstand abrasion, ultraviolet radiation, and other environmental pollutants [10-14]. Baneshi et al. investigated the use of coatings in the design of cool coatings for thermal management applications. In these

*Corresponding author: * nbaran@yildiz.edu.tr, nilbaran@gmail.com

https://doi.org/10.30509/pccc.2026.167804.1509

systems, coatings were designed to reflect the visible (VIS) and near-infrared (NIR) portions of solar radiation and minimize heat transfer into building interiors, thereby reducing cooling energy demand [15]. Jumrus et al. addressed the urgent need for improved thermal management and highlighted the limitations of conventional three-layer coatings in reducing solar heat accumulation [16]. The studies proposed the use of active cooling technologies that dissipated thermal energy into the atmosphere through the 8-13 μm atmospheric window [17, 18]. The authors also emphasized the importance of incorporating superhydrophobic properties with water contact angles above 150°, as such surfaces were highly resistant to environmental degradation. This dual-functional strategy provided self-cleaning and fouling resistance, protecting the cooling performance of coatings against mechanical and chemical damage. Ultimately, the combination of radiative cooling and superhydrophobicity significantly improved energy efficiency and extended the service life of coated surfaces [19-21]. Dullaert et al. examined the physical and chemical factors governing the reflective gloss of dried powder coatings, a critical parameter for industrial aesthetic standards. They also showed that gloss was negatively affected by pigment loading, particularly TiO_2 and $BaSO_4$, when the mass fraction exceeded 45 % [22]. For powder coatings, appearance especially gloss was crucial [23]. Nelson clarified that a notable class of paints used in protective and ornamental coatings consisted of binders cured by the action of air and oxygen [24]. Shirani et al. investigated the development of lightweight alloys such as titanium and aluminum in response to the growing demand for energy-efficient vehicles in automotive and aerospace industries [25]. Despite their favorable strength-to-weight ratios, these materials often exhibited poor tribological performance, characterized by high friction and wear susceptibility [26]. The study explored thermally sprayed coatings applied to cylinder liners as an alternative to conventional steel liners in engine blocks. This approach aimed to reduce overall vehicle weight while maintaining necessary mechanical and thermal protection. The findings highlighted the critical role of surface engineering in overcoming the inherent limitations of lightweight alloys in high-stress applications [27]. Researchers examined the industrial transition from solvent-based coatings to powder coatings as a response to increasingly strict environmental regulations on volatile organic compounds (VOCs) [28-30]. Other studies highlighted the functional advantages of powder coating systems, including superior corrosion and abrasion resistance compared to conventional liquid coatings [31, 32]. This work focused particularly on thermosetting powder coatings (TPCs), which had replaced earlier thermoplastic systems due to improved cross-linking and application performance [33]. By classifying common resin systems such as epoxy, polyester, and hybrid formulations, the studies demonstrated how these materials provided tailored protective and decorative properties. Ultimately, the work emphasized the importance of resin selection in developing sustainable and high-performance protective coatings [34, 35]. Researchers investigated the use of plant oils such as castor, soybean, and linseed oils as sustainable chemical feedstocks. The study highlighted the unique trifunctional nature of castor oil, which contained hydroxyl, unsaturation, and fatty ester groups within its molecular structure [36]. Studies in the literature contributed to the ongoing transition toward eco-friendly polymeric materials [37, 38], as these reactive functional groups enabled the synthesis of a wide range of industrial derivatives [39]. This review examined chemical modification pathways of these oils and identified strategies for replacing petroleum-based polymers. Ultimately, it emphasized the importance of bio-based precursors in achieving sustainable high-performance material systems [40]. Another study addressed the increasing necessity of effective anti-corrosion strategies for both industrial and everyday applications [41], where organic coatings were widely used as cost-effective protective solutions [42, 43]. According to Young's equation, the hydrophobicity of these coatings, represented by the contact angle, was closely related to their performance [44]. Recent studies highlighted that the incorporation of functional polymer architectures and nanostructured materials significantly enhanced both thermal stability and insulation performance in advanced coating systems [45, 46]. Literature demonstrated that epoxy/Al_2O_3 nanoparticle networks formed strong three-dimensional structures that provided excellent mechanical durability and long-term corrosion resistance [47].

Recent research efforts focused on incorporating two-dimensional materials into coating systems to further enhance protective performance. The objective of these studies was to investigate how such materials improved long-term anti-corrosion efficiency and structural integrity in organic coatings [48-51]. A study focused on the complex challenge of achieving “color harmony” in automotive coatings, which relied on combinations of chemical and effect pigments to produce multi-angle optical effects [52].

In this study, the factors and parameters affecting coating performance were investigated, and a highly glossy coating with optical, aesthetic, thermal conductivity, adaptive surface, and morphological performance was developed. The coating was designed to be visually perceptible and optimized accordingly. Contact angle measurements were used to evaluate surface wettability, indicating an increase in surface hydrophilicity with improved wetting behavior. Castor oil and titanium metallic particles were incorporated into the coating system to enhance dispersion and optical brilliance. A systematic approach was applied to ensure controlled preparation and consistent variation in coating composition. By adjusting additive concentrations under constant processing conditions, coating thickness, gloss, color, color difference, and thermal behavior were thoroughly investigated. The methodological approach yielded reliable and consistent results for potential coating applications.

2. Experimantal

White aqueous pigment, castor oil, a titanium-based metallic gloss pigment, epoxy resin, and a hardener were used as the materials in this study. The primary coloring component was the aqueous white pigment, while castor oil was used to evaluate its ability to impart a glossy appearance to the coating system. The titanium-based metallic pigment was employed to provide high opacity, strong tinting strength, and resistance to environmental variations. Additionally, epoxy resin was used to improve the binding properties and enhance the varnish characteristics of the coating formulation.

2.1. Preparation for coating

The samples were prepared by filling 24 beakers with two primary base systems: 12 beakers contained 10 g of white pigment, while the remaining 12 were filled with 5 g of epoxy resin. To improve the workability of the highly viscous resin mixture, 2 g of hardener was added to each epoxy sample to obtain a more homogeneous and processable formulation. All mixtures were mechanically stirred at 300 rpm for 5 min to ensure uniform dispersion of the additives. Subsequently, both the pigment- and epoxy-based systems were subdivided into four equal sets to investigate the effects of different additives, specifically titanium metallic pigment, castor oil, and their combination, using concentration ranges from 1-4 % (Table 1). Coating applications were performed on aluminum substrates using an applicator technique with a controlled wet film thickness of 150 µm. Prior to coating, the aluminum surfaces were cleaned and prepared to ensure proper adhesion. After application, the coated samples were cured in an oven at 60 °C for 15 min. Following the curing process, the coated plates were removed from the oven and allowed to cool to room temperature under ambient conditions to ensure stabilization prior to further characterization. The overall experimental design and formulation details were summarized in Table 1 and illustrated schematically in Figure 1.

2.2. Characterization

The analysis of the instruments used, and their advantages was conducted to evaluate the thermal stability and high-reflectivity performance of the coatings. A multipoint laser infrared thermometer (CEM DT-835) was used for temperature measurements. To evaluate color deviation in the coatings and to determine color differences, a colorimeter (3nh NR60CP) was employed. The morphology of the coating material, gloss distribution, and adaptive surface characteristics were analyzed using a microscope (Bresser DST-1028) to observe the coating morphology and distribution. Simultaneous measurements of temperature differences and weight changes between the samples and reference materials were carried out using a thermal analysis instrument (PerkinElmer Diamond TG/DTA-Seiko Instruments SII, Exstar 6300 TG/DTA). A contact angle goniometer (Biolin Scientific Attension Theta Line) was used to evaluate optimized surface properties and assess surface wettability behavior. The coating thickness on the plates and the differences between coated and uncoated regions were measured using a digital caliper (Insize 1108-150). Finally, the gloss of the coated materials at a measurement angle of 60°, as well as the intensity of reflected light, was measured using a gloss meter (Linshang LS195).

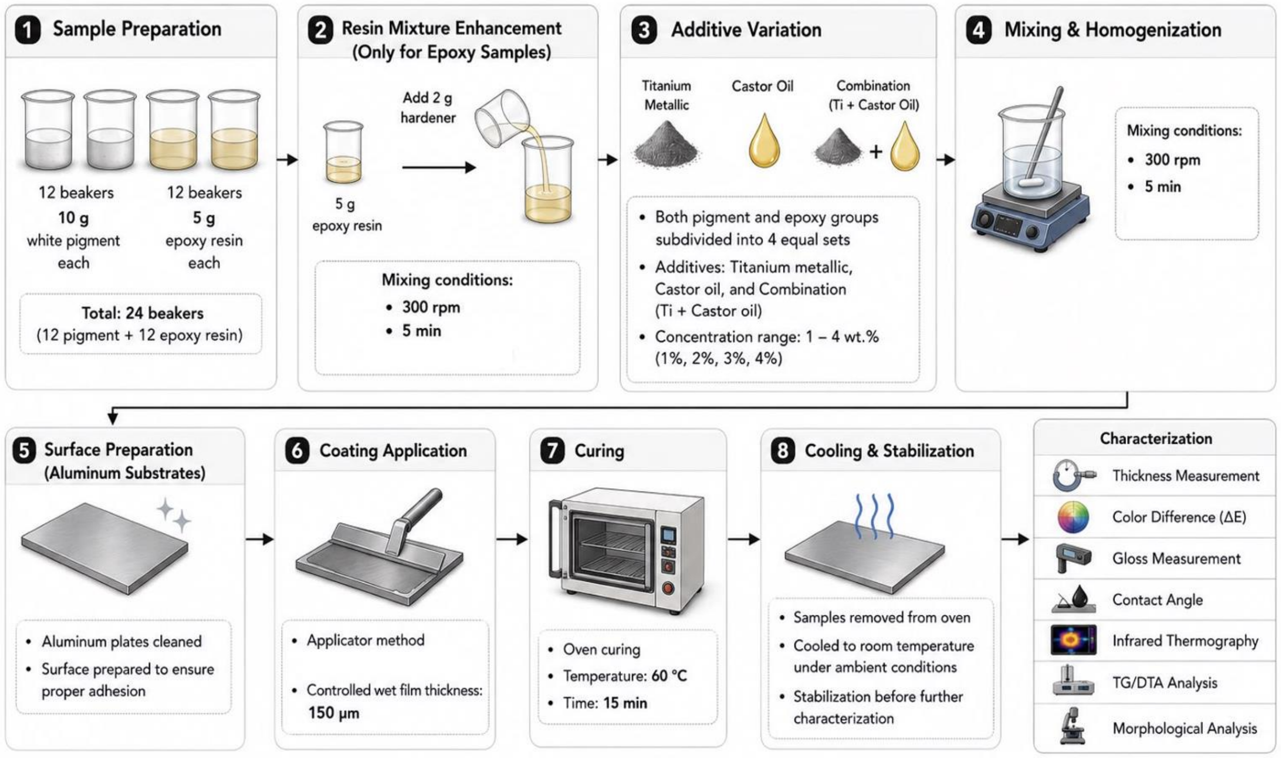

Figure 1: Methodology of the study.

Table 1: Formulation of 24 coating samples prepared with different titanium and castor oil contents.

Sample	Matrix	Base amount (g)	Castor oil (%)	Titanium metallic (%)
S1	White pigment	10	1	1
S2	White pigment	10	2	2
S3	White pigment	10	1	0
S4	White pigment	10	2	0
S5	White pigment	10	0	1
S6	White pigment	10	0	2
S7	White pigment	10	3	3
S8	White pigment	10	4	4
S9	White pigment	10	3	0
S10	White pigment	10	4	0
S11	White pigment	10	0	3
S12	White pigment	10	0	4
S13	Epoxy resin	5	1	1
S14	Epoxy resin	5	2	2
S15	Epoxy resin	5	3	3
S16	Epoxy resin	5	4	4

Table 1: continue.

Sample	Matrix	Base amount (g)	Castor oil (%)	Titanium metallic (%)
S17	Epoxy resin	5	1	0
S18	Epoxy resin	5	2	0
S19	Epoxy resin	5	3	0
S20	Epoxy resin	5	4	0
S21	Epoxy resin	5	0	1
S22	Epoxy resin	5	0	2
S23	Epoxy resin	5	0	3
S24	Epoxy resin	5	0	4

3. Results and Discussion

3.1. Infrared method results

The temperature difference (ΔT) presented in Table 2 between the coating surface and the aluminum substrate was used to evaluate the thermal response and heat distribution behavior of the coated systems under infrared heating conditions. Infrared thermography measurements were performed using a surface emissivity value of $\varepsilon = 0.95$, which was appropriate for polymer-based coating materials. The ΔT values reflected the degree of thermal interaction between the coating layer and the substrate, rather than directly indicating thermal insulation or heat-barrier performance. Higher surface temperatures corres-ponded to increased heat absorption and/or reduced heat dissipation capability of the coating system, whereas lower ΔT values indicated more limited heat accumulation and more efficient thermal equilibration with the substrate. The results showed noticeable variations in ΔT among the samples, particularly within the epoxy-based formulations (samples 20 and 22), which exhibited higher temperature differences compared to the other samples. These variations could be attributed to differences in coating composition, local thickness variations, and dispersion homogeneity, all of which could influence heat transfer pathways at the coating–substrate interface. Therefore, the observed ΔT variations could be interpreted as differences in thermal response behavior and heat distribution characteristics rather than direct evidence of enhanced thermal barrier performance. This distinction was important for correctly understanding the infrared thermography results within the scope of the present study for the materials [53].

Table 2 showed that the highest temperature increase was observed for Sample 22, followed by Sample 2 and Sample 24. The variation could be directly attributed to differences in formulation and matrix composition. Samples 1-12 were based on a white pigment-containing system, where the presence of pigment particles could enhance light scattering and partially affect heat dissipation behavior. In contrast, Samples 13 and onwards were formulated with an epoxy resin matrix, which generally exhibited different thermal response characteristics due to its crosslinked network structure. In particular, Sample 22 and Sample 2, which belonged to the white pigment system with comparable filler loading, exhibited higher $\Delta T = (T_2\text{-}T_1)$ (°C) values, suggesting more pronounced heat accumulation under the tested conditions. The result could be related to reduced thermal conductivity and increased localized energy absorption within pigment-rich regions. On the other hand, Sample 24, despite being part of the epoxy-based system, showed a lower temperature increase, which could be explained by the more homogeneous heat distribution capability of the epoxy network and its comparatively different optical–thermal interaction behavior. Overall, these results indicated that the thermal response was strongly dependent on formulation type, particularly the balance between pigment content, matrix structure, and heat dissipation efficiency.

Table 2: Temperature values for metal surface and coating (S1-S12 white pigment, S13-S24 epoxy resin)

No	Metal, T_1 (°C)	Coating+Metal, T_2 (°C)
1	58.20 ± 0.08	72.20 ± 0.11
2	50.70 ± 0.07	86.70 ± 0.15
3	97.40 ± 0.12	104.30 ± 0.04
4	97.70 ± 0.10	109.40 ± 0.09
5	58.20 ± 0.07	71.40 ± 0.11
6	87.90 ± 0.12	100.30 ± 0.06
7	95.70 ± 0.15	100.40 ± 0.01
8	91.30 ± 0.11	100.70 ± 0.10
9	86.70 ± 0.13	93.60 ± 0.01
10	80.90 ± 0.08	87.20 ± 0.11
11	83.60 ± 0.06	100.30 ± 0.13
12	84.70 ± 0.14	105.20 ± 0.09
13	65.00 ± 0.05	70.60 ± 0.04
14	71.00 ± 0.09	74.50 ± 0.02
15	84.20 ± 0.10	90.00 ± 0.12
16	70.30 ± 0.14	78.50 ± 0.05
17	77.30 ± 0.11	89.90 ± 0.02
18	84.40 ± 0.12	92.60 ± 0.13
19	86.40 ± 0.12	88.50 ± 0.11
20	73.80 ± 0.03	94.50 ± 0.08
21	83.70 ± 0.14	93.40 ± 0.16
22	68.60 ± 0.15	109.40 ± 0.02
23	91.80 ± 0.05	107.90 ± 0.10
24	76.50 ± 0.13	98.90 ± 0.13

3.2. Gloss measurement results

The gloss values measured at 60° showed a clear separation into two distinct groups (Table 3). The first group (samples 1-12) exhibited very low gloss values, ranging approximately from 7.3 to 12.4 GU, indicating matte or low-reflectivity surface characteristics. These results suggested that, in these samples, the surface was not sufficiently smooth or uniform to enable effective light reflection, possibly due to suboptimal coating structure or inadequate film formation. Such low-gloss behavior generally reflected a rougher surface morphology and limited optical performance [54]. In contrast, samples 13-24 demonstrated a significant increase in gloss values, ranging from approximately 63.4 to 115.1 GU. In particular, samples 21 and 22 exhibited the highest values (113.2 and 115.1 GU), indicating highly reflective and glossy surface characteristics. This enhancement in gloss was likely associated with improved surface uniformity, better dispersion of additives, and more effective film formation. Additionally, the presence of specific additives could have contributed to a smoother surface topology and enhanced light reflection, thereby improving the overall optical performance of the coating. The significant improvement suggested that specific formulation conditions strongly enhanced surface smoothness and light reflectivity. Overall, the results showed that the coating system could exhibit both low- and high-gloss behaviors depending on the formulation, with optimized samples achieving superior optical performance.

Table 3: Gloss measurements of each sample coating.

No	Gloss 60°
1	11.5 ± 0.20
2	12.1 ± 0.10
3	10.4 ± 0.15
4	12.4 ± 0.17
5	7.8 ± 0.20
6	9.5 ± 0.13
7	10.1 ± 0.10
8	11.1 ± 0.10
9	9.6 ± 0.09
10	10.7 ± 0.20
11	7.3 ± 0.05
12	7.5 ± 0.13
13	87.4 ± 0.19
14	70.2 ± 0.01
15	63.4 ± 0.14
16	84.4 ± 0.31
17	89.3 ± 0.09
18	89.9 ± 0.07
19	90.3 ± 0.09
20	68.9 ± 0.21
21	113.2 ± 0.19
22	115.1 ± 0.18
23	83.5 ± 0.21
24	66.9 ± 0.31

3.3. Thickness measurement results

Table 4 presented the coating thickness (Δt) between the aluminum plate and the applied coating material. For most pigment-based coatings, a relatively smooth surface was observed, and the measured thickness values were generally uniform across the samples. However, slight variations in coating thickness, when correlated with temperature differences, indicated increased heat absorption in relatively thinner regions. The behavior was attributed to the lower viscosity of the aqueous pigment system, which promoted the formation of thinner layers during application. From a heat transfer perspective, reduced coating thickness [55] decreased the thermal resistance of the system, allowing more efficient heat conduction from the substrate to the surface. Additionally, surface smoothness and thickness uniformity played a critical role in both thermal and optical performance. Minor inconsistencies in thickness could lead to localized variations in heat distribution and energy absorption. Therefore, optimizing viscosity and application parameters was essential to achieve both uniform thickness and improved thermal insulation characteristics. In this context, tm represented the thickness of the base aluminum substrate (mm), while td represented the thickness of the coated sample (mm). The coating thickness difference was calculated as Δt = td-tm (mm). Higher Δt values indicated the formation of thicker coating layers, whereas lower values corresponded to thinner and more compact coating structures.

Overall, the results demonstrated that coating thickness was a key parameter influencing both thermal response and surface properties of the materials. The combined effect of formulation (pigment- or resin-based system) and application behavior significantly affected the final coating structure. In particular, the relationship between thickness variation and thermal performance suggested that even small deviations in Δt could lead to measurable changes in heat transfer and surface behavior. Therefore, controlling coating thickness during application was essential not only for achieving uniform surface quality but also for ensuring consistent functional performance under thermal loading conditions.

To improve measurement reliability, coating thickness values were obtained from repeated measurements (n = 3) using a digital caliper, and the average values were reported. All samples were coated under identical processing and measurement conditions, and therefore the observed differences were primarily attributed to the coating formulations rather than substrate thickness variations.

3.4. Color measurement results

In Table 5, the color differences [52] of the samples affecting the quality of gloss distribution were presented. In the white pigment-based samples, the color difference values were relatively low, whereas the resin-based samples exhibited higher color difference values. Color differences were evaluated using the CIE L*a*b* color space system. The total color difference (ΔE*) between the treated and reference samples was calculated using Eq. 1:

$$\Delta E^*_{ab} = \sqrt{(L^*_2 - L^*_1)^2 + (a^*_2 - a^*_1)^2 + (b^*_2 - b^*_1)^2} \quad (1)$$

Table 4: Measured coating thickness values between reference and coated samples.

No	tm (mm)	td (mm)
1	2.51 ± 0.26	2.67 ± 0.28
2	2.48 ± 0.29	2.68 ± 0.27
3	2.68 ± 0.09	2.79 ± 0.16
4	2.70 ± 0.07	2.86 ± 0.09
5	2.60 ± 0.17	2.74 ± 0.21
6	2.58 ± 0.19	2.78 ± 0.17
7	2.55 ± 0.22	2.76 ± 0.19
8	2.52 ± 0.25	2.69 ± 0.26
9	2.83 ± 0.06	3.10 ± 0.15
10	2.86 ± 0.09	3.02 ± 0.07
11	2.93 ± 0.16	3.17 ± 0.22
12	2.89 ± 0.12	3.06 ± 0.11
13	3.00 ± 0.23	3.24 ± 0.29
14	3.09 ± 0.32	3.20 ± 0.25
15	3.05 ± 0.28	3.21 ± 0.26
16	3.03 ± 0.26	3.23 ± 0.28
17	0.65 ± 0.03	0.80 ± 0.05
18	0.65 ± 0.03	0.77 ± 0.08
19	0.55 ± 0.13	0.78 ± 0.07
20	0.86 ± 0.18	1.00 ± 0.15
21	0.83 ± 0.15	0.95 ± 0.10
22	0.71 ± 0.03	0.95 ± 0.10
23	0.51 ± 0.17	0.76 ± 0.09
24	0.68 ± 0.02	0.79 ± 0.06

The color difference was calculated using the CIE Lab color space model, as expressed in the equation Eq. 1. In the formulation, L* represented the lightness component, while a* and b* denoted the chromaticity coordinates along the green–red and blue–yellow axes, respectively. The subscripts 1 and 2 referred to the reference and measured samples. The reference color was defined as the untreated (control) sample measured under identical conditions. The color differences were calculated by comparing each specimen with the reference sample. Accordingly, ΔL, Δa, and Δb values were determined as the differences between the corresponding L*, a*, and b* coordinates of the specimen and those of the reference. The overall color difference (ΔE^*_{ab}) was obtained between the two-color positions in the CIE L*a*b space. In this study, two reference systems were used for color difference evaluation. The first reference system was the white pigment (organic coating), which was used to evaluate the deviation of modified formulations from the pigment standard. The second reference system was the neat epoxy resin, which was used to quantify the color change induced by the incorporation of pigments and functional additives. All measurements were performed under identical experimental conditions. The ΔE* values represented the overall magnitude of color difference between the tested samples and corresponding reference systems. The calculation followed CIE76 standard color difference method.

3.5. Morphological results

Figure 2 illustrated the morphology of the white pigment modified with castor oil and titanium metallic pigment and revealed significant differences in surface morphology among the samples. Some samples exhibited high gloss and pronounced sparkle effects due to the higher content of titanium metallic pigment, in contrast to the other samples. The variation in surface appearance was closely related to the additive content and its distribution within the coating matrix. The observed morphological features [56] were in good agreement with the gloss measurement results, confirming the consistency between surface structure and optical performance. The microscopic observations reported in a previous epoxy-resin-based study were considered for comparison, since both systems shared the same epoxy matrix despite containing different additives [57].

3.6. Contact angle results

Figure 3 showed that image A represented the reference surface, while image B corresponded to the optimized surface condition. The contact angle decreased from 65.20° (reference surface) to 48.38° (optimized surface), indicating an increase in surface hydrophilicity and improved wettability after surface modification. This reduction in contact angle suggested that the surface modification process effectively increased the surface energy, leading to enhanced interaction with water droplets. The observed trend was found to be consistent with previous studies reported in [58], confirming a wettability behavior. Overall, the optimized surface exhibited higher wettability compared to the reference surface, demonstrating successful tuning of surface properties through the modification process.

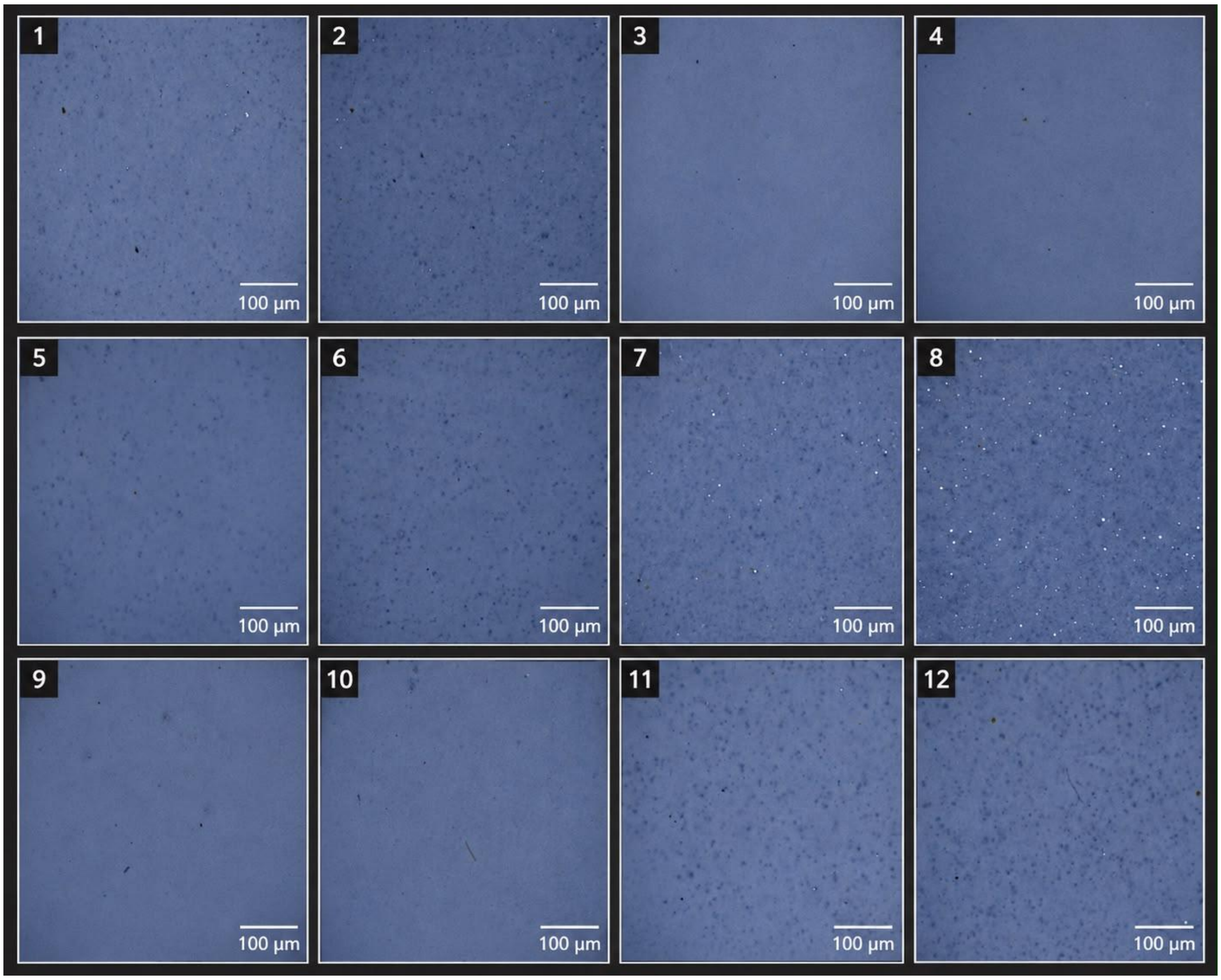

Figure 2: Morphology of each white pigment (70x) (S1-S12).

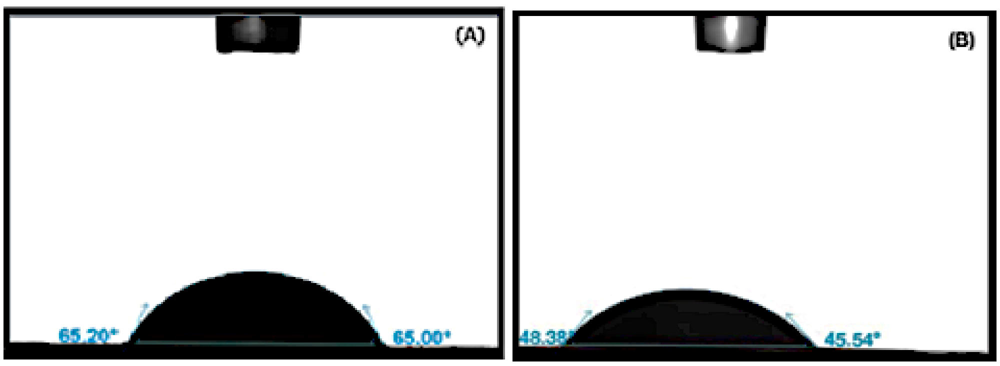

Figure 3: Contact angle measurements of (A) reference and (B) optimum samples.

Table 5: Color distances between white pigment and epoxy resin samples by colorimeter.

No	L*	a*	b*	ΔE*
1	95.00 ± 0.05	-0.73 ± 0.04	0.85 ± 0.03	2.73
2	94.81 ± 0.14	-0.84 ± 0.07	0.58 ± 0.24	3.03
3	96.26 ± 0.31	-0.56 ± 0.21	1.74 ± 0.12	2.19
4	96.39 ± 0.24	-0.42 ± 0.15	1.95 ± 0.13	2.22
5	95.25 ± 0.09	-0.79 ± 0.02	1.06 ± 0.24	2.55
6	94.70 ± 0.25	-0.84 ± 0.07	0.48 ± 0.14	3.12
7	94.91 ± 0.04	-0.91 ± 0.14	0.02 ± 0.10	3.58
8	92.39 ± 0.16	-1.05 ± 0.28	-0.57 ± 0.19	4.72
9	96.14 ± 0.19	-0.55 ± 0.22	1.84 ± 0.02	2.11
10	96.07 ± 0.12	-0.51 ± 0.26	1.92 ± 0.10	2.02
11	93.94 ± 0.01	-0.98 ± 0.21	0.05 ± 0.27	3.55
12	93.57 ± 0.18	-1.06 ± 0.24	-0.10 ± 0.12	3.77
13	73.36 ± 0.20	-3.34 ± 0.13	8.93 ± 0.14	2.32
14	64.90 ± 0.16	-4.31 ± 0.14	9.27 ± 0.27	7.86
15	73.60 ± 0.26	-3.72 ± 0.25	12.91 ± 0.11	6.09
16	76.28 ± 0.12	-4.35 ± 0.18	9.60 ± 0.23	4.67
17	80.73 ± 0.17	-2.64 ± 0.13	5.71 ± 0.19	8.64
18	69.99 ± 0.16	-5.28 ± 0.10	9.51 ± 0.11	3.33
19	71.99 ± 0.13	-4.28 ± 0.12	6.05 ± 0.25	1.01
20	72.64 ± 0.12	-3.94 ± 0.03	5.73 ± 0.17	1.33
21	83.15 ± 0.19	-3.52 ± 0.15	12.07 ± 0.17	12.00
22	83.36 ± 0.20	-2.56 ± 0.07	8.77 ± 0.07	11.20
23	86.97 ± 0.11	-5.11 ± 0.14	8.42 ± 0.18	14.70
24	69.75 ± 0.21	-4.55 ± 0.28	6.26 ± 0.14	2.78

Table 6 showed that the reference sample had very close left and right contact angle values (65.20° and 65.00°), with only 0.10° individual deviation from the group mean. The small deviation indicated that the droplet shape and surface response were relatively uniform on both sides of the reference coating. In contrast, the optimum sample presents lower contact angle values (48.38° and 45.54°), confirming a clear improvement in surface wetting behavior. The mean contact angle decreased from 65.10° for the reference sample to 46.96° for the optimum sample, corresponding to approximately 27.9 % reduction. The decrease suggested that the optimized coating surface became more hydrophilic, probably due to improved surface energy, better additive dispersion, and increased interaction between the water droplet and the coating surface. The slightly higher side-to-side variation in the optimum sample could be related to minor surface roughness or local coating heterogeneity; however, the overall trend clearly supported enhanced wettability compared with the reference coating.

Table 6: Individual deviation values calculated from the sample mean.

Sample	Position	Measured value (°)	Deviation from mean (°)	Value ± individual deviation (°)
Reference sample (A)	Left	65.20	0.10	65.20 ± 0.10
Reference sample (A)	Right	65.00	0.10	65.00 ± 0.10
Optimum sample (B)	Left	48.38	1.42	48.38 ± 0.42
Optimum sample (B)	Right	45.54	1.42	45.54 ± 0.42

3.7. TG/DTA results

Figure 4 showed that the optimal sample exhibited improved thermal stability compared to the reference sample, as evidenced by TG/DTA analysis. The optimal formulation demonstrated a higher residual mass at 600°C, indicating enhanced char formation and reduced thermal degradation. Both samples displayed a similar decomposition peak around 408°C, suggesting comparable primary degradation behavior, while differences in final residue indicated the influence of formulation on thermal stability. The improved thermal resistance of the optimal sample was attributed to the presence of thermally stable inorganic components within the coating structure, which contributed to increased residue formation at elevated temperatures. Overall, these findings demonstrated that the optimized formulation produced a more stable, metal-rich residue, resulting in improved heat resistance and enhanced structural integrity at elevated temperatures. These results, which reflected consistent thermal behavior trends observed in TG/DTA analysis, were found to be in general agreement with those reported in [59].

Table 7 summarized the main TGA parameters, including the degradation onset temperature, offset temperature, DTG peak temperature, maximum degradation rate, and char yield. The optimum sample showed a much higher char yield compared with the reference sample, which exhibited almost complete degradation at the final temperature. The result indicated that the optimum formulation improved the thermal stability and residue formation of the coating system.

3.8. Multi-criteria performance evaluation of the coating

Following the thermal analysis, the overall performance of the coating system was further evaluated in terms of its corrosion resistance, chemical stability, and mechanical properties. The overall performance of the coating system was evaluated using a semi-quantitative 0-5 scoring approach covering corrosion resistance, chemical resistance, and mechanical properties. The results demonstrated that the coating exhibited superior barrier properties against corrosive environments, with a lower corroded surface area compared to the neat epoxy reference. In addition, the coating showed high resistance to organic solvents, including xylene, MEK, and acetone, as well as good stability under acidic and alkaline conditions. Mechanical performance analysis indicated excellent flexibility with no crack formation under deformation, high impact resistance without delamination, and satisfactory surface hardness. The collective results confirmed that the coating system provided a balanced combination of chemical stability, mechanical durability, and corrosion protection performance (Table 8) [60].

Table 7: TGA analysis results including on-set temperature, off-set temperature, and char yield (%) for samples (white pigment).

Sample	On-set temperature (°C)	Off-set temperature (°C)	DTG peak temperature (°C)	Char yield at final temperature (%)
Reference	330	430	408.76	10.0
Optimum	360	445	407.40	48.6

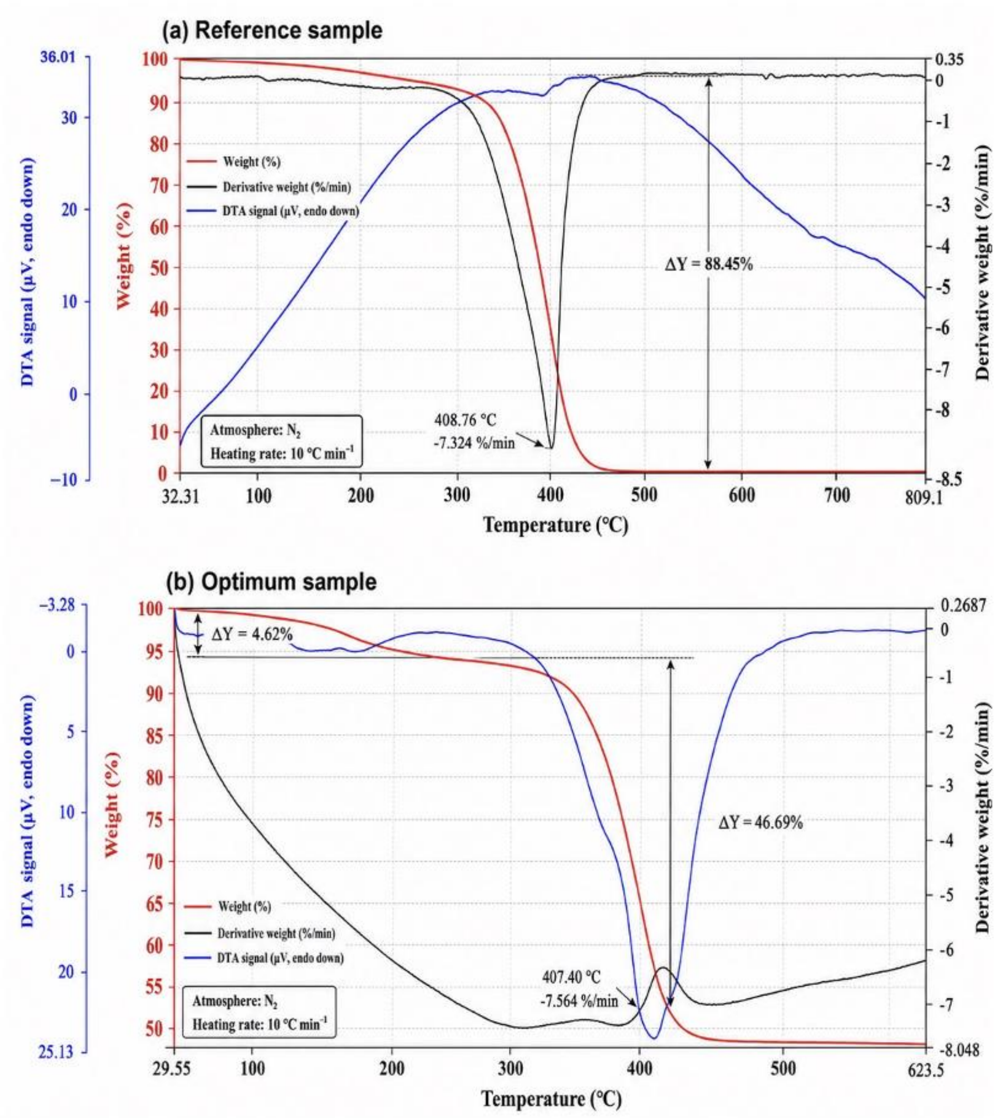

Figure 4: TG/DTA results for reference and optimum samples, respectively.

Table 8: Overall performance assessment of the coating system.

Test	Standard	Evaluation basis	Sample	Result metric	Score (0-5)	Interpretation
Corrosion resistance (salt spray)	ASTM B117	Image-based corroded area (%)	Epoxy resin	12% corroded area	4	High barrier performance
Corrosion resistance (salt spray)	ASTM B117	Image-based corroded area (%)	White pigment system	20 % corroded area	3	Stable surface, no quantified corrosion analysis
Solvent resistance (Xylene, MEK, Acetone)	ASTM D5402	Surface degradation	Epoxy resin	Negligible change	4	High chemical resistance

Table 8: Continue.

Test	Standard	Evaluation basis	Sample	Result metric	Score (0-5)	Interpretation
Solvent resistance	ASTM D5402	Visual observation	White pigment system	No severe degradation	4	Good qualitative resistance
Acid resistance	ASTM D1308	Surface integrity	Epoxy resin	No significant damage	4	Good stability
Acid resistance	ASTM D1308	Surface observation	White pigment system	Minor change	3	Stable trend
Alkali resistance	ASTM D1308	Surface integrity	Epoxy resin	Minor effect	4	Good resistance
Alkali resistance	ASTM D1308	Surface observation	White pigment system	Minor change	3	Stable behavior
Flexibility	ASTM D522	Crack formation	Epoxy resin	No cracks	5	Excellent flexibility
Flexibility	ASTM D522	Visual bending test	White pigment system	No cracking	5	Flexible behavior
Impact resistance	ASTM D2794	Mechanical failure	Epoxy resin	No delamination	4	High impact resistance
Impact resistance	ASTM D2794	Visual observation	White pigment system	No failure	4	Good mechanical integrity
Pencil hardness	ASTM D3363	Scratch resistance	Epoxy resin	2H-3H equivalent	4	Good hardness
Pencil hardness	ASTM D3363	Scratch test	White pigment system	Comparable	4	Satisfactory hardness

4. Conclusion

By incorporating titanium metallic particles and castor oil into an epoxy resin matrix, a multifunctional coating system with improved thermal and surface properties was developed. The results demonstrated that the modified formulations enhanced thermal stability, as confirmed by TG/DTA analysis. The optimal sample exhibited a higher residual mass compared to the reference sample, indicating improved char formation and increased thermal resistance. In addition, surface wettability was affected by the incorporation of additives, as evidenced by the reduction in contact angle from 65.20° to 48.38°, suggesting changes in surface energy and interfacial characteristics. These modifications could contribute to improved coating uniformity and film formation behavior. A relationship between thermal response and surface appearance was also observed. Samples exhibiting lower temperature variations generally showed higher gloss values, indicating that coating composition influences both thermal distribution and optical performance. Overall, this study highlighted the role of formulation design in tailoring the thermal, surface, and optical properties of coating systems. The findings could provide useful guidance for the development of advanced functional coatings with balanced aesthetic and thermal performance.

5. References

1. Zhu M, Huang C, Mao Y. Silica-nanocoated membranes with enhanced stability and antifouling performance for oil-water emulsion separation. Membranes. 2025;15(2): 41. https://doi.org/10.3390/ membranes15020041.
2. Li C, Xia Y, Liu C, Huang R, Qi W, He Z, et al. Lubricin-inspired loop zwitterionic peptide for fabrication of superior antifouling surfaces. ACS Appl Mater Interfaces. 2021;13(35):41978-41986. https://doi.org/10.1021/acsami.1c09254.
3. Cui Y, Sheng M, Liu Y, Feng Y, Li H, Wu Y. Antifouling and self-healing performance of marine coatings based on hydrogen-bond interac-tions. ACS Appl Mater Interfaces. 2023;15(50):58967-58975. https://doi.org/10.1021/acsami.3c 16130.
4. Ma Z, Wu Y, Xu R, Liu Y, Li Z, Liu J, et al. Brush-like organic-inorganic hybrid poly-siloxane surface with omniphobicity and extreme durability. Prog Org Coat. 2021; 154:106171. https://doi.org/10.1016/j.porgcoat. 2021. 106171.
5. Zhang Z, Zhang H, Shao Y, Zhang H, Luo Y, Xu C, et al. Antimicrobial, anti-smudge dual-functional silica coating via interfacial chemical modification. Colloids Surf A Physicochem Eng Asp. 2025; 713:136514. https://doi.org/10.1016/j.colsurfa.2025.136514.
6. Wang C, Chen R, Liu W, Yu J, Liu Q, Liu J, et al. Electron-withdrawing effects for tailoring oxidative-stress-mediated coating in marine antifouling. ACS Appl Mater Interfaces. 2025;17(13):20438-20451. https://doi.org/10.1021/acsami.5c00106.
7. Hao X, Sun Z, Wu S, Wang T, Liu Y, Wu Y, et al. Self-lubricative organic-inorganic hybrid coating with anti-icing and anti-waxing performances by grafting liquid-like polydimethylsiloxane. Adv Mater Interfaces. 2022;9(18). https://doi.org/10.1002/admi.2022 00160.
8. Wang X, Zhang H, Liu B, Man T, Cui X, Liu T, et al. Design, preparation, and tribological properties of novel wide temperature range self-lubricating coatings on TC4 alloy. Surf Coat Technol. 2025; 517:132852. https://doi.org/10.1016/j.surfcoat.2025.132852.
9. Li Z, Liu Y, Liu Y, Ma Z, Pei X, Wu Y, et al. Robustly transparent photothermal icephobic coating via facile in situ PDA polymerization and PDMS brushes grafting. Prog Org Coat. 2025; 210:109717. https://doi.org/10.1016/j.porgcoat.2025.109717.
10. Luo H, Wei H, Wang Z, Li H, Chen Y, Xiang J, et al. Fabrication of UV-curable waterborne polyurethane coatings with self-cleaning, anti-graffiti performance, and corrosion resistance. Colloids Surf A Physicochem Eng Asp. 2023;676:132177. https://doi.org/ 10.1016/j.colsurfa.2023.132177.
11. Guo L, Wu Y, Wang Y, Hu J, Hai O, Liu H, et al. Enhanced efficiency multifunctional coatings for surface protection: The balancing effect of monolithic layered structures. Surf Coat Technol. 2025;517: 132800. https://doi.org/10.1016/j.surfcoat.2025.132800.
12. Gu R, Li X, Mi H, Han J, Zhang C, Liu C, et al. Transparent, robust, and anti-fingerprint silicone coating with a three-dimensional cross-linked network enabled by hydrosilylation reaction. Prog Org Coat. 2024; 196:108749. https://doi.org/10.1016/j.porgcoat. 2024.108749.
13. Liu C, Jiao S, Sun Z, Wang T, Liu Y, Meng X, et al. Development of a hyperbranched oxazolidinone dynamic omniphobic liquid-like coating with high hardness and flexibility. Appl Surf Sci. 2024;654: 159351.https://doi.org/10.1016/j.apsusc.2024.159351.
14. Li Z, Liu Y, Liu Y, Feng K, Li J, Wu Y, et al. Robust transparent photothermal omniphobic coating for efficient anti/deicing and antifogging. ACS Appl Mater Interfaces. 2024; 16(27):35805-35814. https:// doi.org/10.1021/acsami.4c06623.
15. Baneshi M, Maruyama S, Komiya A. The effects of TiO_2 pigmented coatings characteristics on temperature and brightness of a coated black substrate. Sol Energy. 2012; 86(1):200-207. https://doi.org/10.1016/ j.solener.2011.09.019.
16. Jumrus N, Sreejun T, Panthawan A, Maruthappan M, Tippo P, Sanmuangmoon P, et al. Multifunctional self-cleaning, transparency, durability and radiative cooling of H-SiO_2@Lacquer coating for automotive applications. Surf Interfaces. 2025;73:107641. https:// doi.org/10.1016/j.surfin.2025.107641.
17. Meng X, Chen Z, Qian C, Li Q, Chen X. Durable and mechanically robust superhydrophobic radiative cooling coating. Chem Eng J. 2023; 478:147341. https://doi. org/10.1016/j.cej.2023.147341.
18. Wu W, Lin S, Wei M, Huang J, Xu H, Lu Y, et al. Flexible passive radiative cooling inspired by Saharan silver ants. Sol Energy Mater Sol Cells. 2020; 210: 110512. https://doi.org/10.1016/j.solmat.2020.110512.
19. Jumrus N, Chaisen T, Sriboonruang A, Panthawan A, Kumpika T, Kantarak E, et al. A facile methodology to make the glass surface superhydrophobic. Mater Lett. 2020;264:127347.https://doi.org/10.1016/j.matlet.2020. 127347.
20. Jumrus N, Jompaeng J, Panthawan A, Kumpika T, Wiranwetchayan O, Sanmuangmoon P, et al. Transparency and water resistance of a superhydrophobic acrylic surface prepared using THF/IPA etching-assisted SiO_2 NPs. Mater Lett. 2021;304:130618. https://doi.org/10.1016/j.matlet.2021.130618.
21. Jumrus N, Suttanon N, Sroila W, Tippo P, Panthawan A, Thongpan W, et al. Durability and photocatalytic activity of superhydrophobic gypsum boards coated with PDMS/MTCS-modified SiO_2-TiO_2 NPs. Mater Lett.2022;330:133342.https://doi.org/10.1016/j.matlet. 2022.133342.
22. Dullaert K, Steeman P, Bolks J. A mechanistic study of the effect of pigment loading on the appearance of powder coatings. Prog Org Coat. 2011;70(4):205-212. https://doi.org/10.1016/j.porgcoat.2010.07.014.
23. Misev TA. Powder coatings, chemistry and technology. Chichester: Wiley; 1991.

24. Nelson D. Alkyds and polyesters. In: Koleske JV, editor. Paint and coating testing manual. 15th ed. Gardner-Sward Handbook. West Conshohocken (PA): ASTM International; 2012. 65-71.
25. Shirani A, Joy T, Rogov A, Lin M, Yerokhin A, Mogonye J, et al. PEO-Chameleon as a potential protective coating on cast aluminum alloys for high-temperature applications. Surf Coat Technol. 2020; 397:126016. https://doi.org/10.1016/j.surfcoat.2020.126016.
26. Mehran QM, Fazal MA, Bushroa AR, Rubaiee S. A critical review on physical vapor deposition coatings applied on different engine components. Crit Rev Solid State Mater Sci. 2018;43(2):158-175. https://doi.org/10.1080/10408436.2017.1320648.
27. Gérard B. Application of thermal spraying in the automobile industry. Surf Coat Technol. 2006;201(5): 2028-2031. https://doi.org/10.1016/j.surfcoat.2006.04.050.
28. Yuan Y, Chew BT, Yau YH, Qin M, Wan T, Wang Y, et al. Improving the quality of thermosetting powder coatings: A review of the characterization methods, material properties, process techniques, and modeling approaches. Prog Org Coat. 2024;200:108961. https://doi.org/10.1016/j.porgcoat.2024.108961.
29. Chinese Standard. Technical requirement for low-volatile-organic-compound content coatings product. GB/T 38597-2020. Beijing: State Administration of Market Supervision and Administration; 2020.
30. European Parliament and the Council. Directive 2004/42/EC. Limitation of emissions of volatile organic compounds due to the use of organic solvents in certain paints and varnishes and vehicle refinishing products and amending. 2004.
31. Czachor-Jadacka D, Pilch-Pitera B. Progress in development of UV curable powder coatings. Prog Org Coat. 2021;158:106355. https://doi.org/10.1016/j.porgcoat.2021.106355.
32. Czachor-Jadacka D, Biller K, Pilch-Pitera B. Recent development advances in bio-based powder coatings: A review. J Coat Technol Res. 2024; 21 (2):435-444.
33. Du Z, Wen S, Wang J, Yin C, Yu D, Luo J. The review of powder coatings. J Mater Sci Chem Eng. 2016;4(3):54-59. https://doi.org/10.4236/msce.2016.43007.
34. Weiss KD. Paint and coatings: A mature industry in transition. Prog Polym Sci. 1997; 22(2):203-245. https://doi.org/10.1016/S0079-6700(96)00019-6.
35. Golgoon A, Aliofkhazrae M, Toorani M. Nano-composite protective coatings fabricated by electrostatic spray method. Prot Met Phys Chem Surf. 2018;54(2):192-221. https://doi.org/10.1134/S207020511802017X.
36. Doshi VD, Jhalora P. Studies on polyurethane coating based on modified castor oil, commercial acrylate polyols and polysiloxane. Afr J Biomed Res. 2023; 26(3). https://doi.org/10.53555/ajbr.v26i3.7631.
37. Allauddin S, Narayan R, Raju KVSN. Synthesis and properties of alkoxysilane castor oil and their polyurethane/urea-silica hybrid coating films. ACS Sustain Chem Eng. 2013; 1(8):910-918. https://doi.org/10.1021/sc3001756.
38. Shirke A, Dholakiya B, Kuperkar K. Novel applications of castor oil-based polyurethanes: A short review. Polym Sci Ser B. 2015; 57(4):292-297. https://doi.org/10.1134/S1560090415040132.
39. Achaya KT. Chemical derivatives of castor oil. J Am Oil Chem Soc. 1971;48(11):758-763. https://doi.org/10.1007/BF02638537.
40. Akram D, Sharmin E, Ahmad S. Linseed polyurethane/tetraethoxyorthosilane/fumed silica hybrid nanocomposite coatings: Physico-mechanical and potentiodynamic polarization measurements studies. Prog Org Coat. 2014;77(5):957-964. https://doi.org/10.1016/j.porgcoat.2014.01.024.
41. Ma H, Zhang X, Ding Z, Wang Y, Li J, Zhu Y, et al. Epoxy resin coatings with the competitive relationship of hydrophobic and aerophilic towards anticorrosion application. Prog Org Coat. 2026;215:110095. doi: https://doi.org/10.1016/j.porgcoat.2026.110095.
42. K MM, Krishnasamy B, Rajamani A, Muthukaruppan A. Sustainable furfural bis-thymol based benzoxazines: Superhydrophobic, aggregation induced emission and corrosion resistant properties. J Mol Struct. 2024;1322:140495. https://doi.org/10.1016/j.molstruc. 2024.140495.
43. Srinivasan H, Arumugam H, Rimdusit S, Muthukaruppan A. Bio-thymol containing new high-performance thymolphthalein based polybenzoxazine: Thermal, superhydrophobic and dielectric properties. Colloids Surf A Physicochem Eng Asp. 2023;675: 131947.https://doi.org/10.1016/j.colsurfa.2023. 131947.
44. K MM, Arumugam H, Krishnasamy B, Muthukaruppan A. Development of hybrid polybenzoxazine composites from sustainable bio-phenol for dielectric and superhydrophobic water repellent utilizations. Polymer. 2023;283:126287. https://doi.org/10.1016/j.polymer.2023.126287.
45. Seo S, Park J, Park JS, Lee S, Choi D, Kim Y, et al. Polymer donors with hydrophilic side-chains enabling efficient and thermally stable polymer solar cells by non-halogenated solvent processing. Nano Res Energy. 2023; 3(1):2790-8119. https://doi.org/10.26599/NRE.2023.9120088
46. Li Z, Chen Z, Duan Y, Chen J, Yao S, Peng L, et al. A review of silica aerogel based thermal insulation coatings: Preparation, properties and applications. Prog Org Coat. 2025;208:109449. https://doi.org/10.1016/j.porgcoat.2025.109449.
47. Qiao M, Ji G, Lu Y, Zhang B. Sustainable corrosion-resistant superhydrophobic composite coating with strengthened robustness. J Ind Eng Chem. 2023; 121: 215-227. https://doi.org/10.1016/j.jiec.2023.01.025.
48. Chen Z, Li D, Yao S, Duan Y, Chen J, Liu M, et al. Effects of silica aerogel content on the properties of waterborne organic thermal insulation coatings. Gels. 2025;11(7):547.https://doi.org/10.3390/gels11070547.
49. Li Z, Zhou F, Hu M, Liu M, Sun M, Chen Z, et al.

Enhancing thermal safety of hydrophobic SiO_2 aerogels through introducing ammonium polyphosphate intercalated layered double hydroxides. Ceram Int. 2024; 50(14):25895-25907. https://doi.org/10.1016/j.ceramint.2024.04.329.

50. Wang X, Liu Q, Li M, Chen Z, Cheng X, Wu X, et al. Insights into the thermal safety of ambient pressure dried hydrophobic montmorillonite/silica aerogel composites. Ceram Int. 2024;50(4):6135-6145. https://doi. org/10.1016/j.ceramint.2023.11.321.
51. Bai Y, Sun L, Yu Q, Lei Y, Liu B. Biomolecule capturing and sensing on 2D transition metal dichalcogenide canvas. Nano Res Energy. 2022;2: e9120043. https://doi.org/10.26599/nre.2023.9120043.
52. Medina JM, Díaz JA. Classification of batch processes in automotive metallic coatings using principal component analysis similarity factors from reflectance spectra. Prog Org Coat. 2015;88:75-83. https://doi. org/10.1016/j.porgcoat.2015.06.020.
53. Zhang K, Zhang K, Liu B, Lei Y, Guo L, Fu R, et al. An iterative algorithm to improve infrared thermographic systems' accuracy in temperature field measurement of aluminum alloys. Measurement. 2023;210:112547. https://doi.org/10.1016/j.measure ment. 2023.112547.
54. Fletcher T. A simple model to describe relationships between gloss behaviour, matting agent concentration and the rheology of matted paints and coatings. Prog Org Coat. 2002;44(1):25-36. https://doi.org/10.1016/ S0300-9440(01)00206-5.
55. Tan AW, Sun W, Bhowmik A, Lek JY, Marinescu I, Li F, et al. Effect of coating thickness on microstructure, mechanical properties and fracture behaviour of cold sprayed Ti6Al4V coatings on Ti6Al4V substrates. Surf Coat Technol. 2018;349:303-317. https://doi.org/10.1016/j.surfcoat.2018.05.060.
56. Pistofidis N, Vourlias G, Pavlidou E, Patsalas P, Stergioudis G, Polychroniadis E. Study of the structure and morphology of plasma-sprayed tin coating. Surf Coat Technol. 2005;200(22-23):6245-6250. https://doi.org/10.1016/j.surfcoat.2005.11.085.
57. Şahin Fİ, Okumuş Y, Acaralı N. Optimization of color stability in graphene-based hybrid epoxy coatings for aerospace applications utilizing the Box-Behnken design. Prog Color Colorants Coat. 2027;20:13-27. https://doi.org/10.30509/pccc.2026.167770.1496.
58. R AN, Salam JA, Anand AM, Raj A, Jayakrishnan R. Solar cells using spray coated a-axis grown F: SnO_2 thin films. Opt Mater. 2024;159:116612. https://doi. org/10.1016/j.optmat.2024.116612.
59. Parra D, Mercuri L, Matos J, Brito H, Romano R. Thermal behavior of the epoxy and polyester powder coatings using thermogravimetry/differential thermal analysis coupled gas chromatography/mass spectrometry (TG/DTA-GC/MS) technique: Identification of the degradation products. Thermochim Acta. 2002; 386(2):143-151. https://doi.org/10.1016/S0040-6031 (01)00809-7.
60. Ramírez GPM, Byliński H, Niedostatkiewicz M. Mechanical and physical assessment of epoxy, mineral, solvent-based, and water-soluble coating materials. Sci Rep. 2022; 12(1):13647. https://doi. org/10.1038/s41598-022-18022-0.

How to cite this article:
Abdulazeez M, Acarali N. Titanium Metallic Additives for Enhanced Thermal Stablity and Heat Barrier Performance of Bio-based Epoxy for Potential Coating Applications. Prog Color Colorants Coat. 2027;20(2): 221-236. https://doi.org/10.30509/pccc.2026.167804.1509.